Defense Threat Reduction Agency
8725 John J. Kingman Road
MS 6201
Fort Belvoir, VA 22060-6201

DTRA-TR-13-63

TECHNICAL REPORT

Growth and Characterization of Nanostructured Glass Ceramic Scintillators for Miniature High-Energy Radiation Sensors

Approved for public release; distribution is unlimited.

October 2013

HDTRA1-03-D-0009

Mansoor Sheik-Bahae

Prepared by:
OVPR/University Strategic Partnership
MSC02 1660
1 University of New Mexico
Albuquerque, NM 87131

DESTRUCTION NOTICE:

Destroy this report when it is no longer needed.
Do not return to sender.

PLEASE NOTIFY THE DEFENSE THREAT REDUCTION AGENCY, ATTN: DTRIAC/ J9STT, 8725 JOHN J. KINGMAN ROAD, MS-6201, FT BELVOIR, VA 22060-6201, IF YOUR ADDRESS IS INCORRECT, IF YOU WISH THAT IT BE DELETED FROM THE DISTRIBUTION LIST, OR IF THE ADDRESSEE IS NO LONGER EMPLOYED BY YOUR ORGANIZATION.

REPORT DOCUMENTATION PAGE

Form Approved
OMB No. 0704-0188

1. REPORT DATE *(DD-MM-YYYY)*	2. REPORT TYPE	3. DATES COVERED *(From - To)*
00-10-2013	Technical	07/21/2010 - 4/30/2012

4. TITLE AND SUBTITLE

Growth and Characterization of Nanostructured Glass Ceramic Scintillators for Miniature High-Energy Radiation Sensors

5a. CONTRACT NUMBER
HDTRA01-03-D-0009

5b. GRANT NUMBER

5c. PROGRAM ELEMENT NUMBER

6. AUTHOR(S)

Mansoor Sheik-Bahae

5d. PROJECT NUMBER

5e. TASK NUMBER
26

5f. WORK UNIT NUMBER

7. PERFORMING ORGANIZATION NAME(S) AND ADDRESS(ES)

OVPR/University Strategic
Partnership
MSC02 1660
1 University of New Mexico
Albuquerque, NM 87131

8. PERFORMING ORGANIZATION REPORT NUMBER

798B

9. SPONSORING / MONITORING AGENCY NAME(S) AND ADDRESS(ES)

Defense Threat Reduction Agency
8725 John J. Kingman Road
Fort Belvoir, VA 22060
PM/James Reed

10. SPONSOR/MONITOR'S ACRONYM(S)

DTRA

11. SPONSOR/MONITOR'S REPORT NUMBER(S)

DTRA-TR-13-63

12. DISTRIBUTION / AVAILABILITY STATEMENT

Approved for public release; distribution is unlimited.

13. SUPPLEMENTARY NOTES

14. ABSTRACT

Synthesis and characterization of scintillation crystals was performed at the Los Alamos National Lab (LANL). Melt quenching and sol-gel synthesis were applied to prepare various glass ceramic scintillators. For the first time ever, a glass ceramic containing 35 mol% LaF3:Ce3+ was made. Differential scanning calorimetry, x-ray diffraction, transmission electron microscopy, nuclear magnetic resonance, photoluminescence and radioluminescence spectroscopy, and FTIR/Raman spectroscopy and neutron scattering measurements were performed. Temporal dynamics was investigated by ultra-short bursts of XUV radiation at UNM. The rise time was resolved using Kerr gating technique with 8 ps resolution. Spectro-temporal dynamics was resolved using streak camera and tunable pump at second/third harmonic (400/267nm) and XUV. Observed rise time scaling is consistent with chromophore trap dynamics. Rise time of ~80ps in glass ceramics was measured for the first time. Varying plasma parameters as well as excitation pulse characteristics optimized XUV generation efficiency by 40 times compared to standard yield. Combined with improved collection efficiency, newly developed UNM scintillation dynamics lab is now ready for characterization of various scintillators for future material optimization.

15. SUBJECT TERMS

XUV Spectroscopy, Scintillation, Glass Ceramic Scintillators, Ultrafast Spectroscopy

16. SECURITY CLASSIFICATION OF:			17. LIMITATION OF ABSTRACT	18. NUMBER OF PAGES	19a. NAME OF RESPONSIBLE PERSON
a. REPORT	b. ABSTRACT	c. THIS PAGE	UU	23	James Reed
Unclassified	Unclassified	Unclassified			19b. TELEPHONE NUMBER *(include area code)* 703-767-8793

CONVERSION TABLE

Conversion Factors for U.S. Customary to metric (SI) units of measurement.

MULTIPLY →	BY →	TO GET
TO GET ←	BY ←	DIVIDE
angstrom	1.000 000 x E -10	meters (m)
atmosphere (normal)	1.013 25 x E +2	kilo pascal (kPa)
bar	1.000 000 x E +2	kilo pascal (kPa)
barn	1.000 000 x E -28	meter^2 (m^2)
British thermal unit (thermochemical)	1.054 350 x E +3	joule (J)
calorie (thermochemical)	4.184 000	joule (J)
cal (thermochemical/cm^2)	4.184 000 x E -2	mega joule/m^2 (MJ/m^2)
curie	3.700 000 x E +1	*giga bacquerel (GBq)
degree (angle)	1.745 329 x E -2	radian (rad)
degree Fahrenheit	$t_k = (t^\circ f + 459.67)/1.8$	degree kelvin (K)
electron volt	1.602 19 x E -19	joule (J)
erg	1.000 000 x E -7	joule (J)
erg/second	1.000 000 x E -7	watt (W)
foot	3.048 000 x E -1	meter (m)
foot-pound-force	1.355 818	joule (J)
gallon (U.S. liquid)	3.785 412 x E -3	meter^3 (m^3)
inch	2.540 000 x E -2	meter (m)
jerk	1.000 000 x E +9	joule (J)
joule/kilogram (J/kg) radiation dose absorbed	1.000 000	Gray (Gy)
kilotons	4.183	terajoules
kip (1000 lbf)	4.448 222 x E +3	newton (N)
kip/$inch^2$ (ksi)	6.894 757 x E +3	kilo pascal (kPa)
ktap	1.000 000 x E +2	newton-second/m^2 ($N-s/m^2$)
micron	1.000 000 x E -6	meter (m)
mil	2.540 000 x E -5	meter (m)
mile (international)	1.609 344 x E +3	meter (m)
ounce	2.834 952 x E -2	kilogram (kg)
pound-force (lbs avoirdupois)	4.448 222	newton (N)
pound-force inch	1.129 848 x E -1	newton-meter (N-m)
pound-force/inch	1.751 268 x E +2	newton/meter (N/m)
pound-force/$foot^2$	4.788 026 x E -2	kilo pascal (kPa)
pound-force/$inch^2$ (psi)	6.894 757	kilo pascal (kPa)
pound-mass (lbm avoirdupois)	4.535 924 x E -1	kilogram (kg)
pound-mass-$foot^2$ (moment of inertia)	4.214 011 x E -2	kilogram-meter^2 ($kg-m^2$)
pound-mass/$foot^3$	1.601 846 x E +1	kilogram-meter^3 (kg/m^3)
rad (radiation dose absorbed)	1.000 000 x E -2	**Gray (Gy)
roentgen	2.579 760 x E -4	coulomb/kilogram (C/kg)
shake	1.000 000 x E -8	second (s)
slug	1.459 390 x E +1	kilogram (kg)
torr (mm Hg, 0^0 C)	1.333 22 x E -1	kilo pascal (kPa)

*The bacquerel (Bq) is the SI unit of radioactivity; 1 Bq = 1 event/s.

**The Gray (GY) is the SI unit of absorbed radiation.

TABLE OF CONTENTS:

I. ***Synthesis of Nano-Structured Glass Ceramic***

Synthesis of Nano-Structured Glass Ceramic and Characterize Structure and Morphology of Glass Ceramic were performed under a subcontract at Los Alamos National Lab (LANL) under supervision of Dr. Markus Heheln. Upon receiving the funds, LANL team commenced working on the synthesis and characterization of the nano-structured glass ceramics in the second quarter. The LANL team interviewed and hired a postdoc (Dr. Lakshminarayana Gandham, an expert in glass ceramic and crystal growth) who joined the group in February 2011. Dr. Lakshminarayana Gandham is an expert in the synthesis and characterization of rare-earth doped glass ceramics (GC), with over 40 publications in this field. He is currently completing the training required to conduct the research on this project.
The strategy for synthesizing glass ceramics of cerium-doped YAG and LaF_3 has been refined. We explored both melt quenching as well as sol-gel synthesis. The melt quenching technique has been used previously to achieve our preliminary results with undoped LaF_3 glass ceramics as well as micron-sized YAG:Ce glass ceramics. We will refine this technique to produce the nano-structured materials for this project. Sol-gel synthesis is an alternative technique that allows preparation at significantly lower temperatures and yields samples that tend to have superior homogeneity. This method will be pursued in parallel as it may provide higher quality samples that are easier to manufacture.

Our LANL collaborators completed all the required training at LANL to carry out my research work on LaF_3:Ce and YAG:Ce doped nanoglass ceramics as scintillators both by sol-gel and melt-quench technique (using high temperature furnace). We have carried out the experiments on LaF3:Ce doped glass ceramics with different mol ratio of LaF_3/Ce by using the sol-gel process for which the "sols" are under gelation for 4 weeks. Also the same composition LaF_3:Ce doped glass ceramics are under preparation by using the melt-quench method. In addition, to investigate the effect of nucleating agent, such as TiO_2 on the LaF_3:Ce doped glass ceramics the respective "sols" incorporated with Titanium isopropoxide as TiO2 precursor is also prepared and were under gelation process for 4 weeks. These glass ceramics doped with TiO_2 were also prepared by melt-quench method for comparison with sol-gel samples performance through structurally, and optically. In the process of preparing the YAG:Ce doped glass ceramics, the respective glass ceramics "sols" were prepared by using sol-gel method and went under 'geletion" process. The same composition YAG:Ce doped nanoglass ceramics were prepared by melt-quench method also after successful preparation of LaF3:Ce, and LaF_3:Ce with TiO_2 doped nanoglass ceramics.

We have succeeded in preparing, for the first time ever, a glass ceramic containing 35 mol% LaF_3:Ce^{3+}. Previous studies reported in the literature achieved LaF_3 concentrations of <10 mol%, and these materials were not Ce^{3+} doped. The high LaF_3:Ce^{3+} concentration achieved here is essential for maximizing the volume fraction of scintillator in the glass ceramic material. This is a breakthrough and creates a material platform for subsequent application-specific optimization.
The general glass composition is 50% SiO_2 – 15% Al_2O_3 – 35% LaF_3 (mol%) doped with CeF_3 and Sb_2O_3. In a first step, the material is prepared as an amorphous glass by melting of the starting materials, quenching of the melt, and annealing of the glass. In a second step, in-situ LaF_3:Ce^{3+} crystallization is induced by heat treatment near the material's crystallization temperature to obtain the transparent glass ceramic. Three major difficulties had to be overcome in the synthesis of these glasses and glass ceramics:

1. Published procedures for LaF_3-containing aluminosilicates of this kind turned out to be flawed and not workable. Therefore, a synthesis method had to be developed from scratch, which included optimization of the glass composition, melting temperature, melting time, crucible material, atmosphere, and annealing temperature.

2. Melting in ambient air caused undesired oxidation of Ce^{3+} to Ce^{4+}, which is spectroscopically inactive (does not scintillate). This oxidation could be largely prevented by melting under argon atmosphere and by adding Sb_2O_3 as a reducing agent, which acts according to $Ce^{4+}+Sb^{3+}\rightarrow Ce^{3+}+Sb^{4+}$.

3. Sb_2O_3 doped glasses synthesized under argon atmosphere showed a different crystallization behavior than non-Sb_2O_3-doped glasses made under air. This required development of a new crystallization procedure.

Eight SiO_2–Al_2O_3–LaF_3–Sb_2O_3–CeF_3 samples with Ce^{3+} concentrations of 0, 2.5, 4.9, 7.4, 9.8, 12.1, 14.5, 16.8 mol% were fabricated. The compositions are shown in Table 1. A small quantity of Sb_2O_3 was added at a fixed Sb_2O_3:CeF_3=1:4 mol ratio. Melting took place at 1450 ^oC under argon gas flow in covered alumina crucibles. Melting times ranged from 44 to 26 minutes, depending on the composition, and the melt was quenched between two copper plates. The resulting glasses were annealed at 450 ^oC (5 hours) and 525 ^oC (6 hours). Subsequently, the heavily Ce^{3+}-doped samples were heat treated at 740 ^oC (4 hours) and 820 ^oC (4 hours), while the lightly Ce^{3+}-doped glasses were heat treated at 780 ^oC (4 hours) and 800 ^oC (4 hours). The resulting glass ceramics were light yellow in color and translucent.

Table 1: *Nominal composition (in mol%) of SiO_2–Al_2O_3–LaF_3–CeF_3–Sb_2O_3 glass ceramics. A small amount of Sb_2O_3 in the mol ratio Sb_2O_3:CeF_3=1:4 was added to suppress oxidation of Ce^{3+} to Ce^{4+}.*

Sample	SiO_2	Al_2O_3	LaF_3	CeF_3
1	50	15	35	0
2	50	15	32.5	2.5
3	50	15	30	5.0
4	50	15	27.5	7.5
5	50	15	25	10
6	50	15	22.5	12.5
7	50	15	20	15
8	50	15	17.5	17.5

Then we focused on the sol-gel route to produce oxide glasses with a high concentration of LaF_3 and CeF_3. Several series of samples were slowly "dried" at moderate temperatures (<200 ^oC) to affect the formation of a gel. Indications are that our recent adjustments to the synthesis procedure were successful in preventing premature crystallization. These samples were then heated at higher temperatures to induce the formation of a glass and subsequently a glass-ceramic.

II. *Characterize Structure and Morphology of Glass Ceramic*

At LANL, we have an extensive array of characterization techniques at our disposal that we will apply to the synthesized glass ceramics. This includes differential scanning calorimetry (DSC), x-ray diffraction (XRD), transmission electron microscopy (TEM), nuclear magnetic resonance (NMR), photoluminescence and radioluminescence spectroscopy, and FTIR/Raman spectroscopy. In addition, we used neutron scattering at Los Alamos Neutron Science Center (LANSCE), which will provide complementary and highly valuable information on the glass ceramic structure at the nanoscale.

We initiated a comprehensive structural and spectroscopic characterization of the samples shown in Table 1. This includes x-ray diffraction (XRD), energy dispersive x-ray spectroscopy (EDAX), nuclear magnetic resonance (NMR), scanning electron microscopy (SEM), X-ray photoelectron spectroscopy (XPS), differential scanning calorimetry (DSC), absorption spectroscopy, photo luminescence and excitation spectroscopy (PL, PLE), excited state lifetimes, Fourier transform infrared spectroscopy (FTIR), and Raman spectroscopy.

The preliminary results of the structural characterization are presented in the following. Figure 2 shows a representative XRD pattern of a SiO_2-Al_2O_3-LaF_3-CeF_3-Sb_2O_3 glass ceramic. There are two broad peaks due to diffuse scattering in the amorphous glass network as well as a set of sharp diffraction peaks that are completely indexed as a pure LaF_3 crystalline phase. A preliminary analysis of the LaF_3 linewidth indicates that the LaF_3 crystallites are approximately 15 nm in size. Assuming a LaF_3 index of refraction of 1.62 (at 380 nm), a glass matrix index of ~1.55, and a LaF_3 volume fraction of ~50%, an optical scattering length of ~10 cm is calculated for this 15 nm LaF_3 particle size. This is consistent with the translucent appearance of the samples and is essential for future scintillator applications. Figure 2 shows an EDAX spectrum of the glass ceramic containing 17.5 mol% Ce^{3+}. The spectrum indicates that LaF_3 and CeF_3 were both quantitatively incorporated into the alumino-silicate glass. Also visible are the lines associated with the main glass components Si, Al, and O as well as the Sb reducing agent. Figure 3 shows DSC scans of all seven Ce^{3+} doped glasses. The respective glass transition temperature (Tg), crystallization temperatures (Tc), and melting temperatures (Tm) were derived from these scans and are summarized in Table 2. This thermal data will allow us to further optimize the crystallization procedure for the individual glasses.

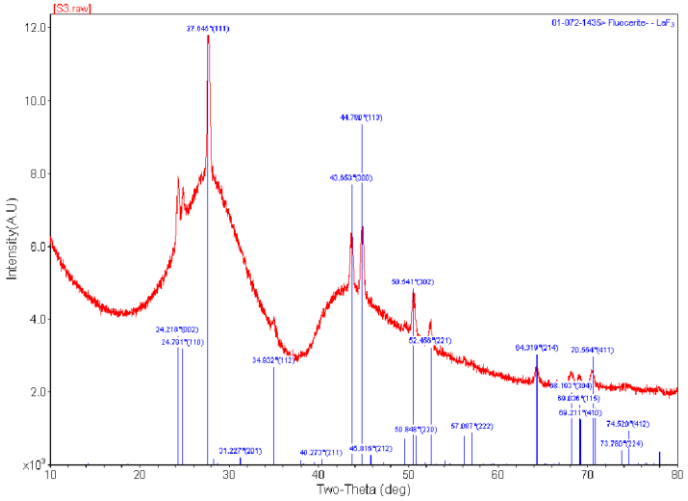

Figure 1: *XRD of a SiO_2-Al_2O_3-LaF_3-CeF_3-Sb_2O_3 glass ceramic (red) and theoretical LaF_3 diffraction lines (blue).*

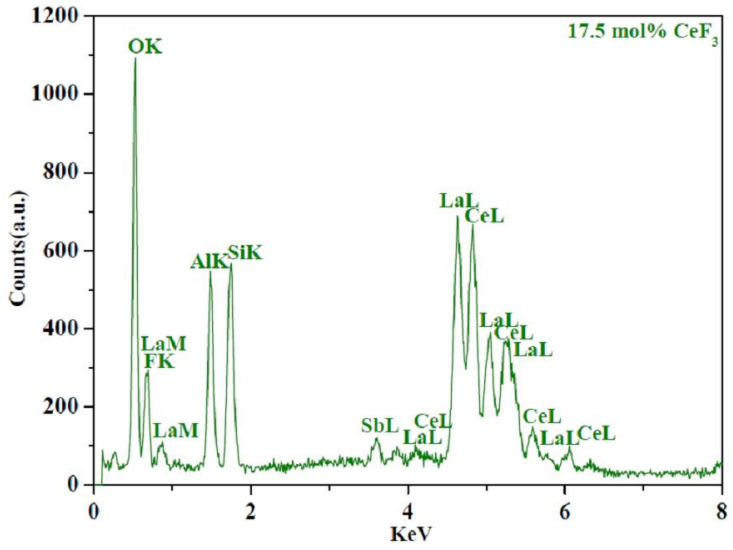

Figure 2: *EDAX spectrum of SiO_2-Al_2O_3-LaF_3-CeF_3-Sb_2O_3 glass ceramic (17.5 mol% Ce^{3+}). The labels "K", "L", and "M" denote the respective group of x-ray emission lines.*

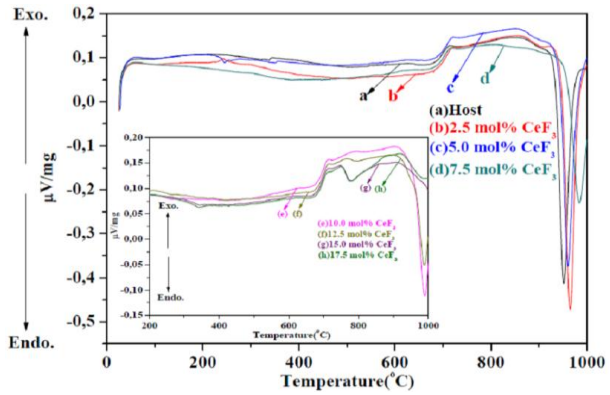

Figure 3: *DSC scans of Ce^{3+}-doped SiO_2-Al_2O_3-LaF_3-CeF_3-Sb_2O_3 glasses.*

Table 2: *Thermal properties of SiO_2-Al_2O_3-LaF_3-CeF_3-Sb_2O_3 glasses.*

CeF_3 concentration (mol %)	T_g(°C) (± 1) °C	T_{c1} (± 0.5) °C	T_{c2} (± 0.5) °C	T_{c3} (± 0.5) °C	T_m (± 0.5) °C
0	641	715	851	…….	952
2.5	639	720	861	…….	965
5.0	655	718	855	…….	961
7.5	661	717	…….	…….	983
10.0	644	713	793	907	990
12.5	654	712	768	903	989
15.0	641	713	749	884	……..
17.5	644	710	750	900	……..

We have performed radio-luminescence (RL) spectroscopy on Ce^{3+}-doped oxyfluoride aluminosilicate glasses and glass-ceramics made by heat-treating the glassed. The glass-ceramics contain nano-crystalline LaF_3:Ce^{3+} in an alumino-silicate glass matrix. We observed that the RL spectrum of the glass-ceramic was similar to that of the corresponding glass. This indicates that the x-ray excited luminescence of the LaF_3:Ce^{3+} nano-crystals is re-absorbed and re-emitted by residual Ce^{3+} in the glass matrix. This should manifest as an increase in the RL photon yield. An experiment is currently underway to measure the absolute photon yield of both the glass and the glass-ceramic to determine if the presence of LaF_3:Ce^{3+} nano-crystals causes a useful enhancement of the scintillator photon yield.

a) *Structural and Optical Characterization of Cerium-doped SiO_2-Al_2O_3-LaF_3 Glasses*

Table 3 summarizes the compositions of the 8 CeF_3-doped SiO_2-Al_2O_3-LaF_3 glasses that were prepared. We have since completed a comprehensive structural and spectroscopic study of these glasses. A respective manuscript has been written and submitted to *Optics Express* where it is currently in review [G. Lakshminarayana, E.M. Weis, B.L. Bennett, A. Labouriau, D.J. Williams, J.G**.** Duque, M. Sheik-Bahae, M.P. Hehlen, "Structural, thermal, and luminescence properties of oxyfluoride glasses highly doped with cerium fluoride", Optics Express, (2012), *submitted*.]

The amorphous nature of the glasses was confirmed by x-ray diffraction, scanning electron microscopy, and Raman spectroscopy. The prepared glasses retained the high nominal fluoride content during melting and showed an actual rare-earth fluoride content of 21-12 mol % as measured by EDS (see Table 4). FTIR spectroscopy identified good complexation between the glass former SiO_2 and chief intermediate Al_2O_3, and both characteristic SiO_4 and AlO_4 units were present in the glass matrices. This was also confirmed by the ^{29}Si, ^{27}Al, and ^{19}F MAS-NMR measurements. The glasses were found to have a T_g of 639-661 °C, indicating a relatively high thermal stability. All of the Ce^{3+}-doped glasses showed intense violet-blue $5d \rightarrow 4f$ emission (402–407 nm) upon direct optical excitation of Ce^{3+} at 335 nm (PL, see Fig. 1) as well as upon excitation with x-rays (RL, see Fig. 2). The integrated luminescence intensity was highest for the 7.5 mol % CeF_3-doped

sample in both PL and RL. The decay lifetime of the excited states was used to identify quenching processes of the Ce^{3+} 5*d* excited state. At higher CeF_3 concentrations, the luminescence intensity decreased, and a fast component in the 5*d* excited-state decay transients gained in magnitude (Table 5). Both concentration quenching via ion-ion interactions and radiative energy transfer were found to be active in the highly CeF_3-doped glasses.

The SiO_2-Al_2O_3-LaF_3 glass composition and synthesis method reported here enable oxyfluoride aluminosilicate glasses with exceptionally high rare-earth fluoride content as well as good chemical and thermal properties. These glasses show promise as low-cost γ-ray scintillators when doped with Ce^{3+}, and they may find applications in the fields of solid-state lighting and quantum cutting when doped with other rare-earth ions.

Table 3: *Nominal composition (in mol%) of SiO_2–Al_2O_3–LaF_3–CeF_3–Sb_2O_3 glass ceramics. A small amount of Sb_2O_3 in the mol ratio Sb_2O_3:CeF_3=1:4 was added to suppress oxidation of Ce^{3+} to Ce^{4+}.*

Sample	SiO_2	Al_2O_3	LaF_3	CeF_3
1	50	15	35	0
2	50	15	32.5	2.5
3	50	15	30	5.0
4	50	15	27.5	7.5
5	50	15	25	10
6	50	15	22.5	12.5
7	50	15	20	15
8	50	15	17.5	17.5

Table 4. *Measured and nominal elemental composition data of (i) host glass (sample 1), (ii) 10 mol % CeF_3 (sample 5), and (iii) 17.5 mol % CeF_3 (sample 8) doped glasses (the x-ray line designations are given in parentheses). Antimony (Sb) was not measured by EDS and was excluded from both the nominal and measured composition.*

	Element	Wt%	At%	Nominal At%
(i)				
	O(K)	31.85	53.66	39.6
	F(K)	12.24	17.36	28.9
	Al(K)	11.68	11.67	8.2
	Si(K)	11.41	10.95	13.7
	La(L)	32.83	6.37	9.6
(ii)				
	O(K)	30.54	54.14	40.3
	F(K)	9.23	13.78	28.5
	Al(K)	11.25	11.83	8.1
	Si(K)	12.74	12.87	13.5
	La(L)	25.35	5.18	6.8
	Ce(L)	10.90	2.21	2.7
(iii)				
	O(K)	15.54	46.18	40.8
	F(K)	3.87	9.69	28.3
	Al(K)	6.22	10.96	8.1
	Si(K)	5.80	9.82	13.4
	La(L)	31.93	10.93	4.7
	Ce(L)	36.63	12.43	4.7

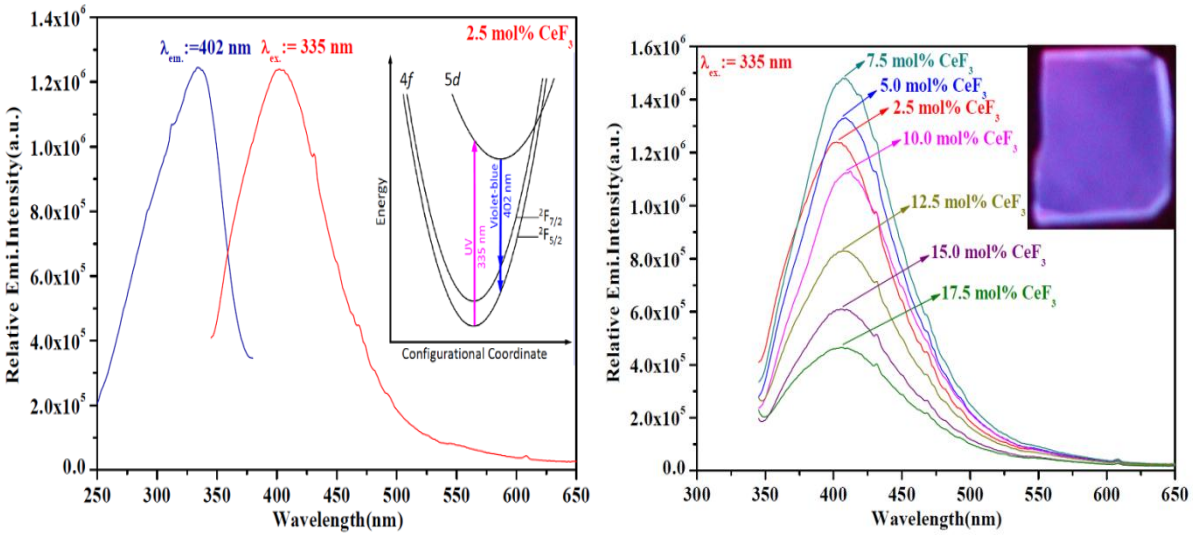

Fig. 4. *Left: PLE and PL spectra of 2.5 mol% CeF_3 doped glass (inset shows the corresponding energy level scheme) Right: PL spectra of all the CeF_3 doped glasses (inset shows photograph of 7.5 mol% CeF_3 doped glass under UV light irradiation).*

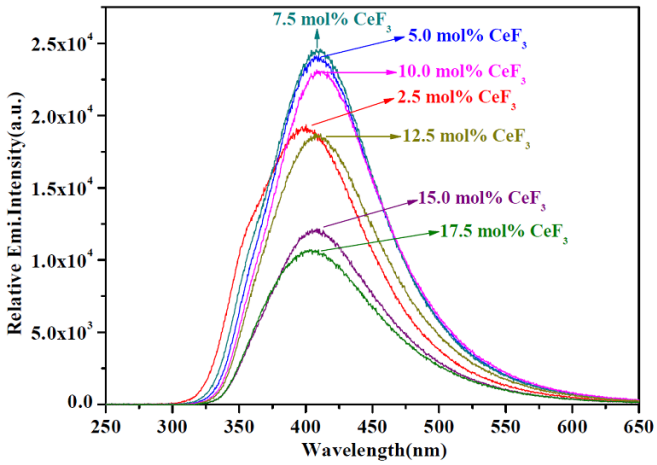

Fig. 5. *Radioluminescence (RL) spectra of all the CeF_3 doped glasses.*

Table 5. *Decay lifetime data of some of the CeF_3 doped glasses.*

CeF_3 concentration (mol %)	Slow component		Fast component	
	τ_s (ns)	Magnitude, A_s	τ_f (ns)	Magnitude, A_f
2.5	34.3 ± 0.44	83.7%	5.8 ± 0.63	16.3%
7.5	34.6 ± 0.48	81.3%	7.3 ± 0.70	18.7%
12.5	32.3 ± 0.62	71.7%	6.4 ± 0.52	28.3%
17.5	29.5 ± 0.52	61.0%	5.8 ± 0.27	39.0%

b) ***Structural and Optical Characterization of Cerium-doped SiO_2-Al_2O_3-LaF_3 Glass Ceramics***

The glass ceramics obtained from heat-treating the glasses shown in Table 3 are currently being thoroughly characterized. In particular we are focusing on separating the emission from Ce^{3+} in the glass matrix (see Fig. 4) from the emission of Ce^{3+} in the LaF_3 nano-crystals, which is at shorter wavelength.

c) ***Structural Study of SiO_2-Al_2O_3-LaF_3 Glasses using Neutron Scattering***

We were granted beam time in early December 2011 at the Los Alamos Neutron Scattering Center to perform a study of the crystallization dynamics of the SiO_2-Al_2O_3-LaF_3 glasses We studied the pure SiO_2-Al_2O_3-LaF_3 glass (sample 1 in Table 3) as well as a SiO_2-Al_2O_3-LaF_3 glass with a small amount of zirconium oxide (ZrO_2), which is known to induce nucleation sites and to promote crystallization. The sample was inserted into a furnace in the neutron beam, and neutron diffraction patterns were measured in 20-minute intervals as the sample was held at the crystallization temperature. The large amount of data from this in-situ crystallization measurement is pending analysis in the first half of 2012. A preliminary analysis indicates that the ZrO_2-doped glass formed LaF_3 crystals more quickly than the pure SiO_2-Al_2O_3-LaF_3 glass, as expected. The detailed analysis will probe for differences in particle size and crystalline volume fraction in the two materials.

III. *Measure Scintillation Transients by XUV Spectroscopy*

Initial experiments on scintillation dynamics were performed using ultrashort laser pulses at λ=400 nm. These experiments employed a conventional photomultiplier tube (PMT) to investigate the scintillation dynamics. These detectors with ~2 ns response time can only shed light on the luminescence fall time and will not resolve the ultrafast rise time in these materials. We will use Kerr-gating to resolve the rise time.

a) *Ultrafast Kerr Gating*

One of the initial ideas that we perused was to perform a pump probe experiment to measure scintillation rise time with high resolution The technique is called Kerr gating. A new ultrafast Kerr gating arrangement was setup. Liquid carbon disulfide (CS_2) was used as the nonlinear medium for measurements. We demonstrated self-gating of the control pulse (from the high power Ti:sapphire laser) and determined the time resolution of the gate to be about 8 picoseconds (see Figure 6).

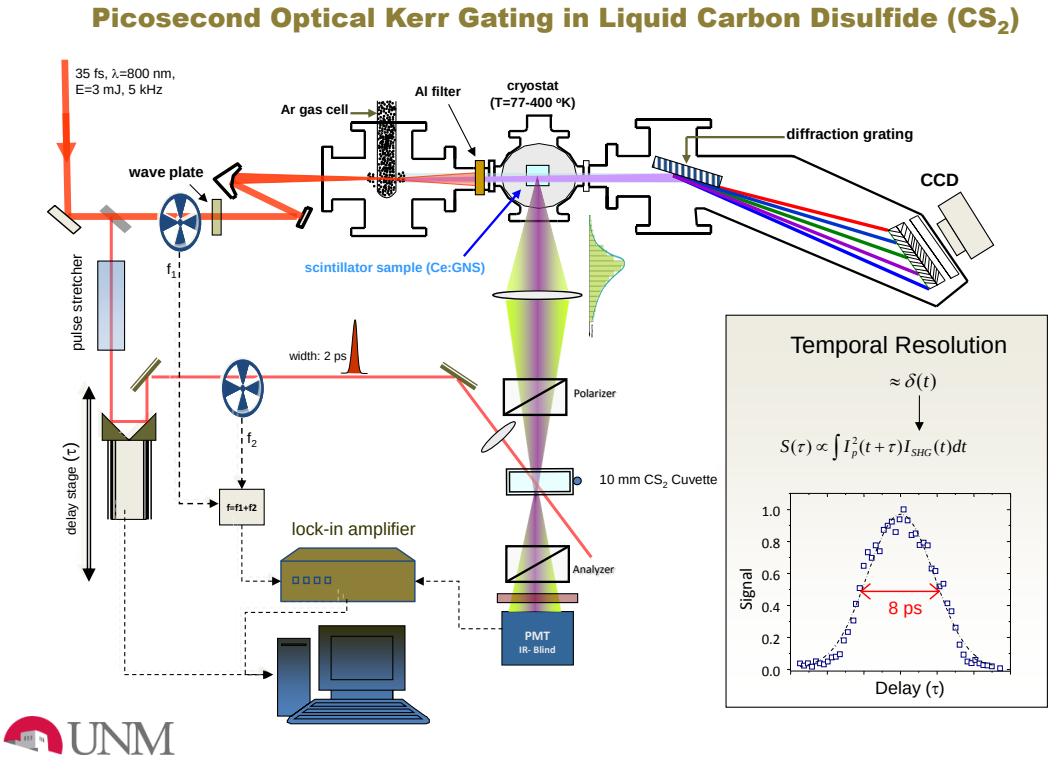

Figure 6. *XUV generation and Kerr gating setup*

Initial studies on fluorescent filters and standard scintillators excited by 2nd and 3rd harmonics of the pump laser show that this technique is successful in resolving the sub nanosecond emission risetime. When excited by XUV pulses, however, the signal-to-noise ratio needs to be improved due to scarcity of photons emitted. We will address this by devising more efficient collection optics, better rejection of the background pump that eventually leaks into the detector, and improve detection sensitivity. Another possibility was to generate XUV more efficiently.

Efficiency improvements was accomplished by pursuing various options in parallel, including two-color excitation, second-harmonic excitation, Using different gas and gas tube/nozzle and optical and gas pressure optimization. Regarding the latter approach, we have switched to a larger diameter gas tube for XUV generation. Using a larger tube provides a longer propagation path through the gas, which will increase the efficiency if properly phase matched. It also becomes easier to align. Using a nozzle on the other hand, makes

alignment and optimization for two-color XUV generation easier while increasing efficiency. Optimum pressure inside the tube is between 70-72 torrs. An improvement of nearly 2-3 fold has been obtained. Prior to implementing this scheme, we optimized the focusing geometry and obtained a 2-3 fold enhancement as shown below:

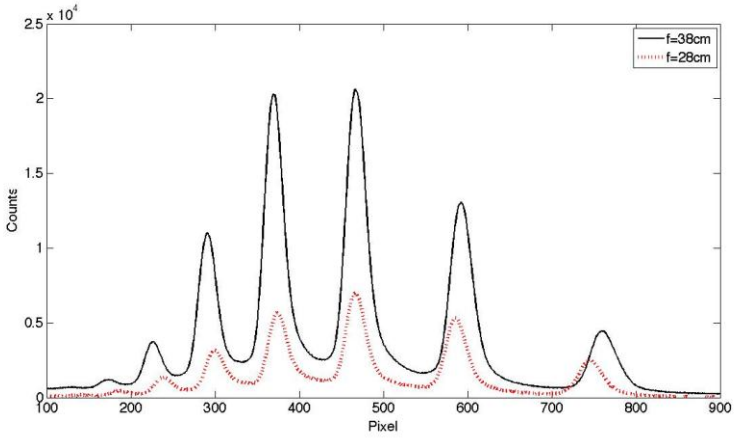

Figure 7. *An enhancement of 2-3 is obtained by performing optimum focusing geometry.*

By using a longer focal length, the Rayleigh distance of the beam at the focus is made larger, thus making the effective interaction length larger.

After optimizing gas pressure, optical alignment and pulse energy we used Xenon for XUV generation for the same conditions. Figure 8 shows Higher Harmonics for Argon and Xenon and Figure 9 illustrates the area under the spectrum, which indicates an increase in efficiency for Xenon.

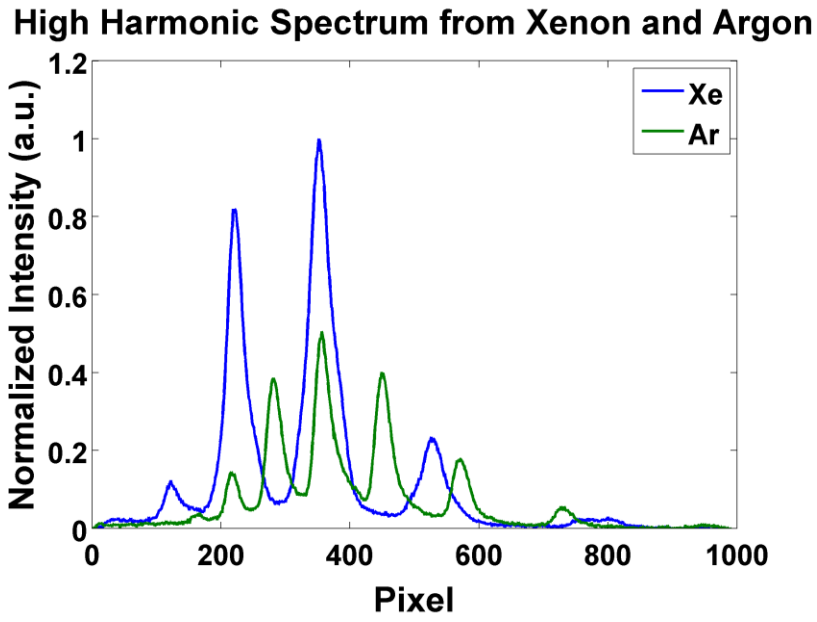

Figure 8. *HHG spectrum from Xenon (Blue) and Argon (Green)*

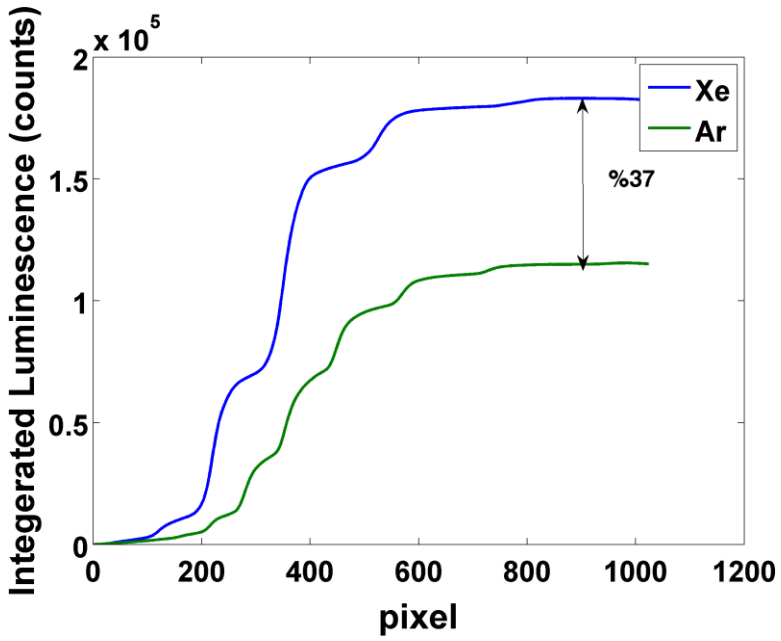

Figure 9. *Integrated Luminescence of High Harmonics from Xenon (Blue) and Argon (Green)*

The XUV generation efficiency using standard method of high-harmonic generation (HHG) is rather small (~10^{-8}). To enhance this efficiency, a number of techniques have been employed. A recent theory by the MIT group [J. Phys. B: At. Mol. Opt. Phys. 44 (2011) 045601] presents a simple analytical expression, and gives simple scaling laws for the efficiency:

$$\eta = 0.0107 \frac{\sqrt{2I_p}\omega_0^5 |a_{rec}|^2 |g(\Delta k, L)|^2}{E_0^4 \Omega^2 \sigma^2(\Omega)} \frac{1-\beta^{4(N-1)}}{(1-\beta^4)N} \left| 1+\beta\, e^{i\pi\left(1-\frac{\Omega}{\omega_0}\right)} \right|^2 \times \left| \frac{a(tb_s)\, a(ta_s)\sqrt{w(E(tb_s))}}{\sin(\omega_0 tb_s)\left[\omega_0(ta_s - tb_s)/(2\pi)\right]^{3/2}} \frac{e^{-i(\bar{S}_s - \Omega ta_s)}}{\sqrt{\left|\partial_t^2 S_s\right|}} + \frac{a(tb_l)\, a(ta_l)\sqrt{w(E(tb_l))}}{\sin(\omega_0 tb_l)\left[\omega_0(ta_l - tb_l)/(2\pi)\right]^{3/2}} \frac{e^{-i(\bar{S}_l - \Omega ta_l - \frac{\pi}{2})}}{\sqrt{\left|\partial_t^2 S_l\right|}} \right|^2$$

Without going into details of each term in the above equation, the parameter of interest to us at this time is ω_0 which is the pump laser frequency. The predicted ω_0^5 scaling suggests that if we use second harmonic (at $2\omega_0$), the efficiency will be enhanced 32 fold. Assuming a 20%-30% efficiency in the second harmonic generation (SHG), an overall enhancement of 6-10 fold can be expected. We are therefore working towards testing this enhancement scheme by generating $2\omega_0$ using a thin BBO crystal as shown below:

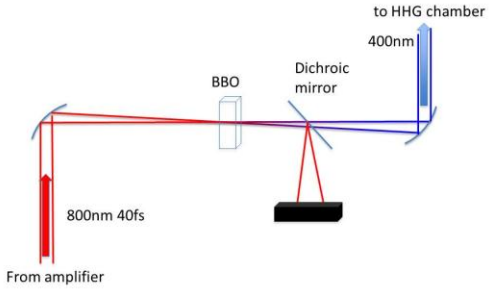

Figure 10. *Generation of second-harmonic (at $2\omega_0$) using BBO crystal as an input to the XUV generation should enhance the output by 10 fold.*

In our quest for more efficient XUV via the process of high harmonic generation (HHG) we took necessary steps and purchased required parts for two-color and second harmonic HHG. The set-up diagram is shown in Figure 11.

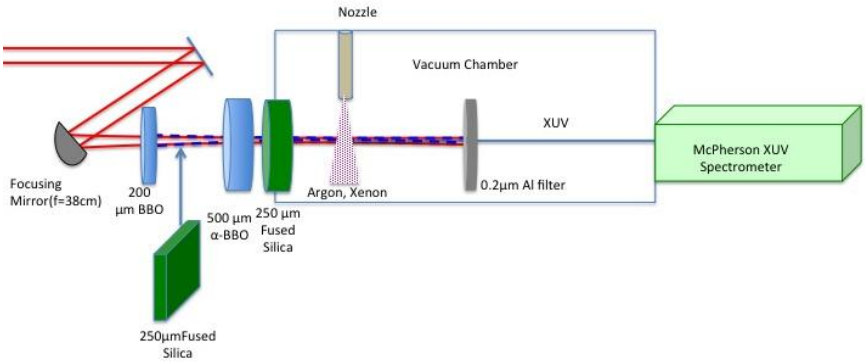

Figure 11. *Experimental set-up for implementing coherent 2-color (ω and 2ω) excitation for improving the HHG efficiency. Laser pulse at fundamental frequency ω (λ=800 nm) generate second harmonic (2ω) in the first BBO. The α-BBO is used to compensate group velocity walk-off between the two pulses introduced by the glass window. Another fused silica plate is used to control the relative phase between the two beams.*

The initial results were quite promising as nearly a 10 fold enhancement was observed. We are currently working on further optimization of this process.

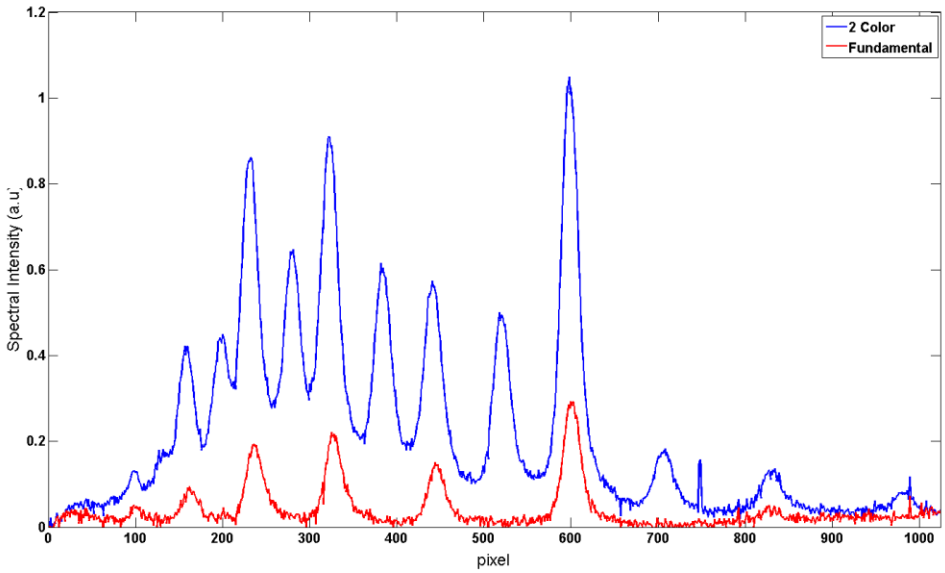

Figure 12. *HHG spectrum under excitation by the 2-color (blue) and fundamental only (red). Nearly a 10-fold enhancement is observed.*

The coherent control and the overall all enhancement of this process is also illustrated in Figure 13. where the integrated HHG signal is measured versus the phase difference between ω and 2ω beams ($\Delta\phi=\phi_{2\omega}-2\phi_{\omega}$).

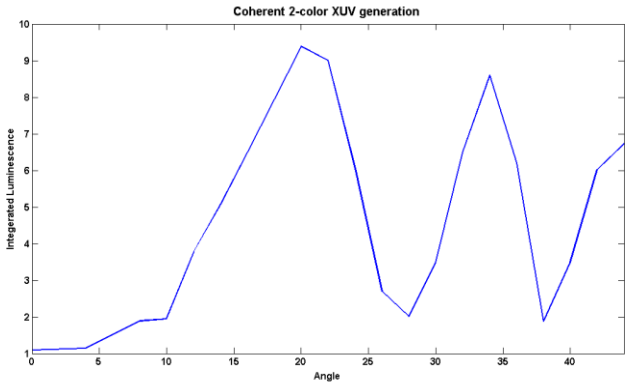

Figure 13. *HHG integrated signal as a function of angle of fused silica phase-plate indicating coherent nature of HHG process as a function of* $\Delta\phi = \phi_{2\omega} - 2\phi_{\omega}$.

b) Time Resolve spectroscopy

Since ultrafast Kerr gating technique was not sensitive enough for low yield scintillators, we decided to measure the scintillation spectral dynamics using an ultrafast photon-counting streak camera. Such a system is however very expensive (~$150k, thus out of our budgetary capacity). Luckily, we managed to get one on loan from Hamamatsu Inc. as they found the application of using their system for studying scintillator dynamics under ultrafast XUV bursts very novel and interesting. This system is shown in Figure 14.

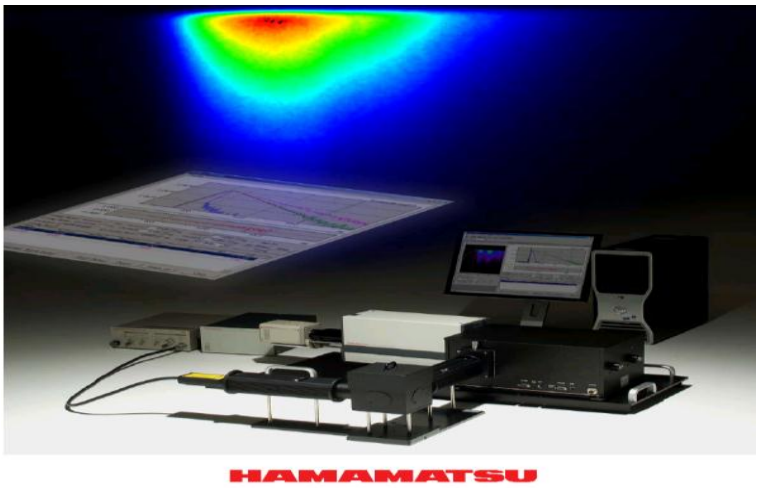

Figure 14. *The C10627 Hamamatsu Streakscope, on loan to UNM for Aug-Sep 2011.*

The Hamamatsu Streakscope (Model C10627) combined with a Princeton instrument spectrometer is one of the best combinations for measuring fluorescence life times and spectral properties of scintillators. This systems temporal resolution can be as low as 15ps. We used this system to study scintillation dynamics of various crystals.

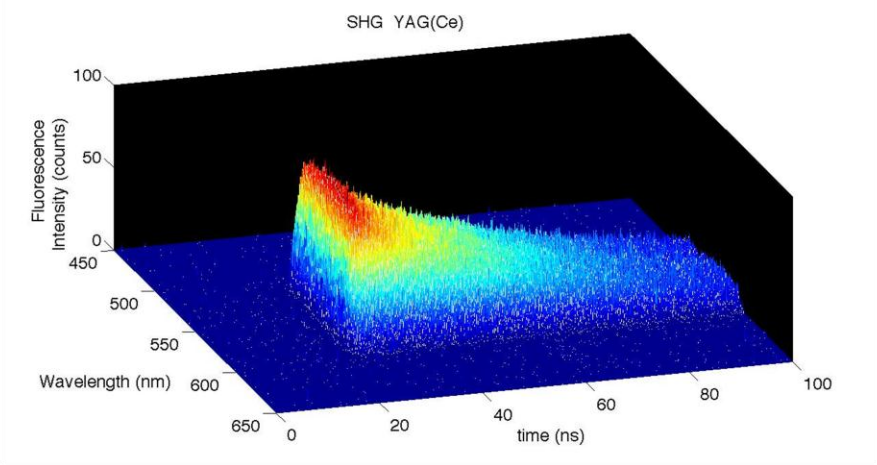

(a)

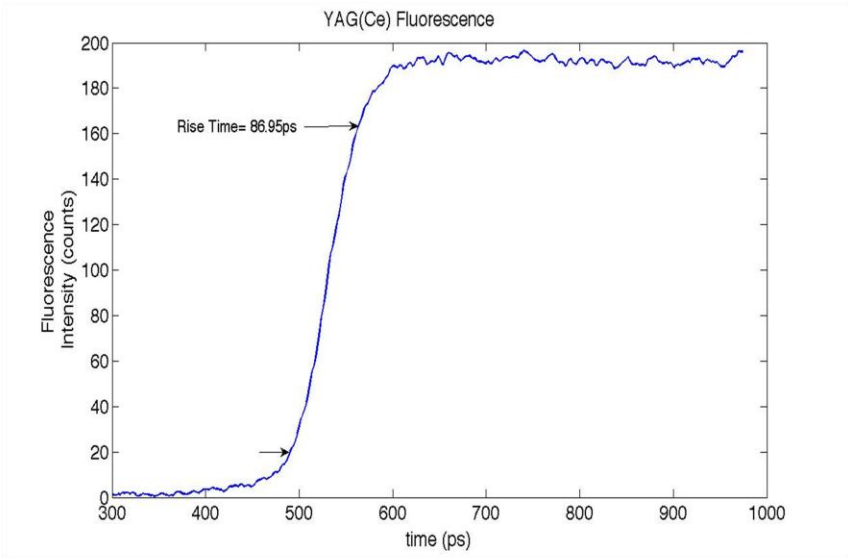

(b)

Figure 15. *YAG(Ce) spectral and temporal fluorescence intensity excited by second harmonic (400nm) (a) Temporal fluorescence intensity averaged over the spectrum (b).*

Figure 12 shows spectral and temporal characteristics of YAG(Ce) glass ceramic excited by second harmonic(400nm) with a fast rise time and broad spectrum which makes it an interesting crystal to study with our XUV source. GNS (Ce) is another scintillator we have tested so far. Fluorescence intensity was measurable when excited by 400nm.The results are illustrated in Figure 3. Initial attempts to resolve temporal properties of YAG(Ce) and GNS(Ce) have not been successful even though we are generating more XUV.

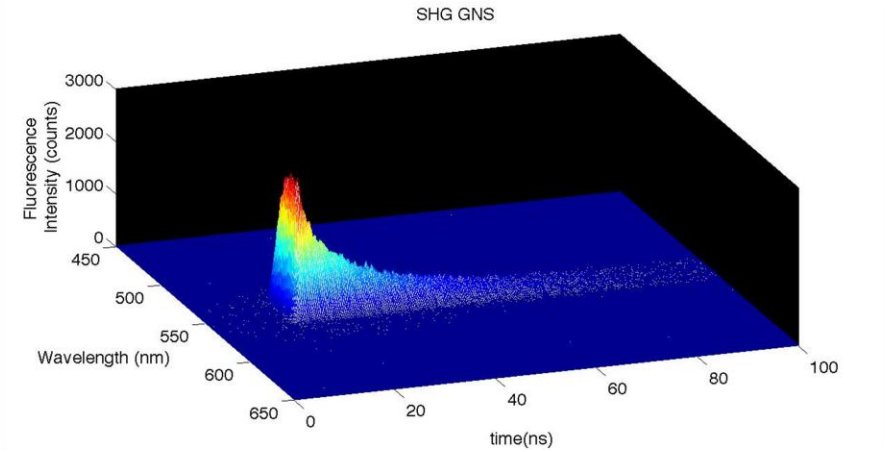

(a)

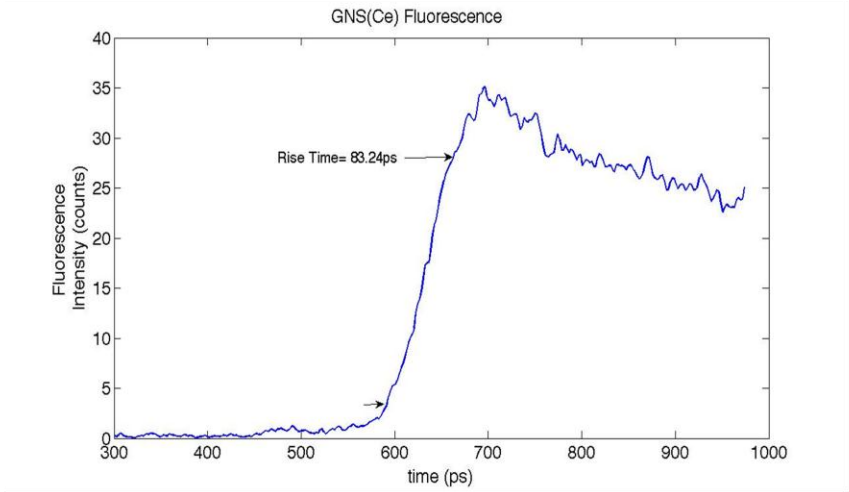

(b)

Figure 16. *GNS(Ce) spectral and temporal fluorescence intensity excited by second harmonic (400nm) (a) Temporal fluorescence intensity averaged over the spectrum (b).*

Looking at CsI(Tl) which is one of the most efficient scintillators we were able to see a small number of fluorescence photons when excited by XUV (Figure 17). As it is apparent from Figure 17 even after counting photons for 10000 seconds we only have 10 counts keep in mind this is for he most efficient scintillator that we have and its not a crystal we are really interested in (because of its slow response).

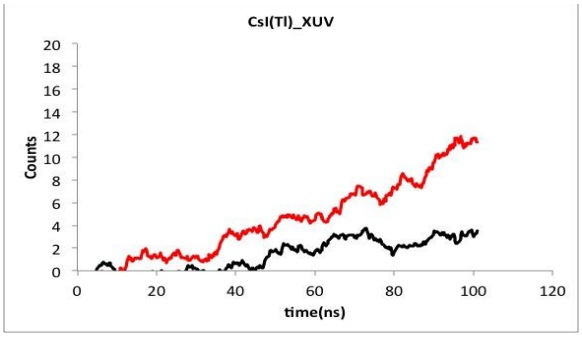

Figure 17. *Photon counting CsI(Tl) fluorescence excited by XUV 10000 photon counts(red) 1000 photon counts (black).*

In order to increase sensitivity of our measurement system we have to improve our fluorescence light collection by removing the spectrometer and changing our collection optics, possibly using fiber bundles very close to the crystal to guide more and more photons towards the streakscope. By removing the spectrometer we will be able to eliminate the 40% loss due to grating efficiencies and using fiber bundles could increase the number of collected photons by an additional 50% or more. Better collection combined with our efforts to increase the XUV generation efficiency can potentially help us understand the behaviors of different crystals regardless of their efficiency and we can provide more accurate assessments to LANL for future crystal synthesis.

We had to return the streak camera to Hamamatsu. Fortunately our collaborators from Los Alamos National Labs have found a very similar Hamamatsu streak camera that we can borrow for a year. This would give us enough time to study the crystals we have (CaF2(Eu), CsI (pure),YAG (Ce), GNS (Ce)) as well as new crystals that will be made in LANL.

C) Fluorescence Collection

As mentioned earlier, using fiber bundles and light pipes could increase the number of collected photons by an additional 50% or more. In order to obtain this level a collection system was designed and it was made by Fiber Tech Optica (see Figure 18), which consists of:

-Silica rod collector in flange with adjustable Z axis
-Optical relay
-Spot-to-2D array bundle
    Spot end: Stainless steel ferrule
    Active area diameter: ~4.4mm
    2D array end: Brass cylindrical ferrule, 18 mm OD x 75 mm long
    Array dimension: 0.98mm width x 15.18mm height
-Sheathing: Black PVC-monocoil tubing

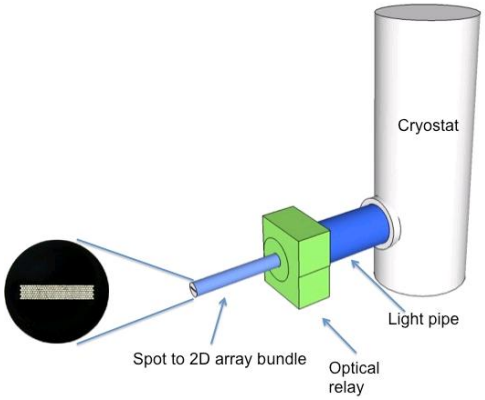

Figure 18. *Use of high numerical aperture fiber-bundle collection assembly for more efficient of coupling scintillation light into the streak camera,*

This collection system has now arrived and is being assembled into the system (See Fig. 20). It will be used with Hamamatsu streak camera that we have borrowed from our Los Alamos National Labs collaborators. The combination will enable us to collect and detect more photons.

Figure 20. *Scintillation-collection fiber-bundle to be integrated with the streak-camera.*

IV. *Conclusion*

Synthesis and characterization of scintillation crystals was performed at the Los Alamos National Lab (LANL). Melt quenching and sol-gel synthesis were applied to prepare various glass ceramic scintillators. For the first time ever, a glass ceramic containing 35 mol% LaF_3:Ce^{3+} was made. Previous studies reported concentrations of <10 mol%, and these materials were not Ce^{3+} doped. The high LaF_3:Ce^{3+} concentration achieved here is essential for maximizing the volume fraction of scintillator in the glass ceramic material. The general glass composition is 50% SiO_2 – 15% Al_2O_3 – 35% LaF_3 (mol%) doped with CeF_3 and Sb_2O_3**.** Differential scanning calorimetry, x-ray diffraction, transmission electron microscopy, nuclear magnetic resonance, photoluminescence and radioluminescence spectroscopy, and FTIR/Raman spectroscopy and neutron scattering measurements were performed. In order to further expand our knowledge about scintillation dynamics crystals were excited by ultra-short bursts of XUV radiation and spectroscopy was done on the samples. These ultra-short bursts of XUV are generated through the process of High Harmonic Generation (HHG) in noble gas. Scintillation rise time was resolved using Kerr gating technique with 8 ps resolution. Spectro-temporal dynamics was resolved using streak camera and tunable pump at second/third harmonic (400/267nm) and XUV. Observed rise time scaling is consistent with chromophore trap dynamics. Rise time of ~80ps in glass ceramics was measured for the first time. Varying plasma parameters as well as excitation pulse characteristics optimized XUV generation efficiency by 40 times compared to standard yield. Combined with improved collection efficiency, newly developed UNM scintillation dynamics lab is now ready for characterization of various scintillators for future material optimization.

Journal Publications:

Gandham Lakshminarayana; Eric M Weis; Bryan L Bennett; Andrea Labouriau; Darrick J Williams; Juan G Duque; Mansoor Sheik-Bahae; Markus P. Hehlen, "Structural, thermal, and luminescence properties of cerium-fluoride-rich oxyfluoride glasses" *Accepted for publication* in the **Journal of Optical Materials** (http://www.journals.elsevier.com/optical-materials/)

DEPARTMENT OF DEFENSE

DEFENSE THREAT REDUCTION
AGENCY
8725 JOHN J. KINGMAN ROAD
STOP 6201
FORT BELVOIR ,VA 22060
ATTN: J. REED

DEFENSE TECHNICAL
INFORMATION CENTER
8725 JOHN J. KINGMAN ROAD,
SUITE 0944
FT. BELVOIR, VA 22060-6201
ATTN: DTIC/OCA

DEPARTMENT OF DEFENSE CONTRACTORS

EXELIS, INC.
1680 TEXAS STREET, SE
KIRTLAND AFB, NM 87117-5669
ATTN: DTRIAC